ACS OMEGA

http://pubs.acs.org/journal/acsodf

Article

Synergetic Catalytic and Photocatalytic Performances of Tin-Doped $BiFeO_3$/Graphene Nanoplatelet Hybrids under Dark and Light Conditions

Sabeen Fatima and Syed Rizwan*

Cite This: *ACS Omega* 2023, 8, 3736−3744

Read Online

ACCESS | Metrics & More | Article Recommendations

ABSTRACT: Because of a rapidly growing need for water, it is essential to find new fast and reliable ways of water purification from organic pollutants. For removing organic azo dyes from water, various catalysts and photocatalysts have been designed to meet crucial water needs. In this study tin (Sn) doped bismuth ferrite (BFO) nanoparticles have been synthesized using the sol−gel technique. Further, BFSO/GNP nanohybrids were synthesized by mixing BFSO nanoparticles with graphene nanoplatelets (GNPs) via a simple and cost effective coprecipitation process. XRD and SEM showed that BFSO/GNP nanohybrids are well grown in crystal structure along with uniform and homogeneous morphology. XPS supported the elemental composition and interface bonding of both materials present inside the nanohybrids. DRS and catalytic activities showed that BFSO/GNP nanohybrids are both dark and light active species for performing dye degradation activities during water purification. The as-synthesized nanohybrids provided efficient dye removal from water even in the absence of light owing to the presence of defects and trap-state carriers (electrons) inside the graphene sheets. The optimized nanohybrid BFSO-15/GNP showed 100% dye removal in 60 min with 90% catalytic activity under dark. The recyclability test showed stable and repeatable performance of BFSO/GNP nanohybrids up to 10 cycles of catalytic activities.

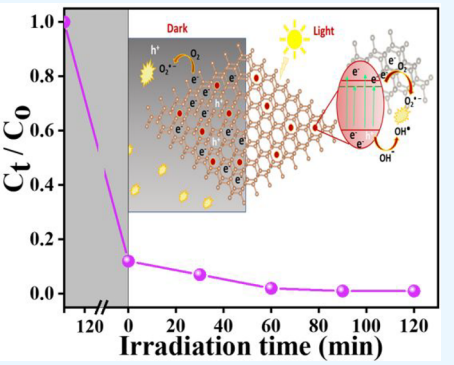

INTRODUCTION

The rapid growing population in today's world is also causing an accelerated industrial growth, because of which organic dye consumption is rapidly increasing day by day.[1] The removal of these colored pollutants from water is a real challenge for researchers, as these dyes bond strongly with the water molecules and are carcinogenic for human life. The removal of these toxic elements from water is usually followed by photocatalysis. The photocatalysis is a light driven phenomenon in which ultraviolet (UV), infrared (IR), or visible light is used to activate the purification process in semiconducting photocatalysts, and as a result of these chain reactions carbon dioxide (CO_2) and water (H_2O) are formed as end products.[2] The catalytic by-products are harmless to human life and can further be processed for water splitting (H_2 fuel generation) and CO_2 reduction phenomenon. The expanding need of water is creating an urgency in the scientific field to purify water in a shorter period to meet the world's water requirements. With this a new field of catalysis emerges in which researchers are designing the catalysts that no longer need light to perform their action for water purification.[3] These materials can start catalytic reactions even in the dark for the removal of organic pollutants. Hence, water can be purified even in the night time when there is no sun and can be provided to the population during day time.[3,4]

The first ever semiconducting photocatalysts in this field were titanium oxide (TiO_2) and zinc oxide (ZnO), having band gaps in the range of 3.2 eV−3.4 eV.[5,6] These materials were UV light active and played their role in removing organic dyes including Congo red (CR), methylene blue, and methylene orange as well as benzidine under light irradiation.[7−9] All these azo dyes have been excessively used by industries since ancient times, and they are difficult to separate from water molecules. So, a need to design visible light driven photocatalysts resulted. The sun is an abundant light source on earth and can be used to purify water on a large scale in a very economical cost-effective way.[10] Hence, with the band gap tuning of initial semiconductors, bismuth ferrite ($BiFeO_3$/BFO) became a fascinating candidate in the photocatalysis field.[11,12] BFO belongs to the perovskite ABO3 type multiferroic materials with a band gap of 2.01 eV.[13] The exceptional characteristics of this material made it a potential candidate in many scientific applications.[14−16]

Received: August 4, 2022
Accepted: September 28, 2022
Published: January 18, 2023

https://doi.org/10.1021/acsomega.2c04971
ACS Omega 2023, 8, 3736−3744

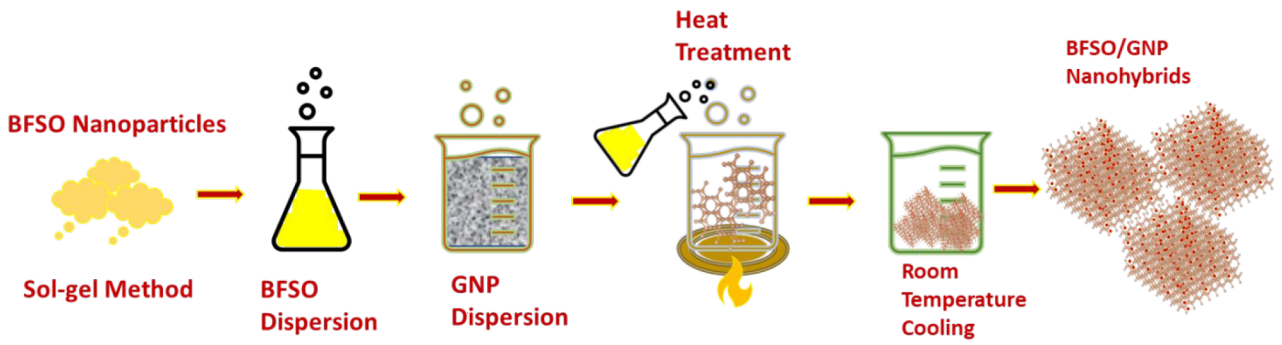

Figure 1. Synthesis scheme for BFSO/GNP nanoplatelets.

Further it has been proven that, with doping, the bandgap of these materials can be modified to perform an efficient photocatalytic activity.[17−19] Different ions have been doped inside the A and B sites of BFO to compensate for the challenges related to defects (Bi and O vacancies) as well as Fe ions valence fluctuations. Among these Tin (Sn^{4+}) has also been investigated to reduce the overall leakage current of the BFO structure and to improve its magnetic moment.[20] The substitution of Sn at B sites of BFO can satisfy the Fe fluctuations and vacancies to improve the overall electrical properties.[21] Also Sn addition inside BFO acts to modify its band gap and makes it a good photocatalyst under visible light.[22]

Graphene on the other hand is also a two-dimensional (2D) material which has been proven to be an excellent photocatalyst upon making heterojunctions or hybrid structures with other materials.[23−26] Different oxides and other 2D structures on combining with the graphene provided enhanced photocatalytic and photocurrent responses in the literature.[27−30] The graphene enhanced surface area and metallic character facilitate the carrier mobility as well as strengthen the photoresponse of the material toward light or electric field.[30] Fast and high performance photocatalysts must possess the essential characteristics of a suitable band gap for absorbing visible light, low carrier recombination rate, and high surface area for increased carrier activity toward active sites of catalysts, for which new and improved heterojunctions have been extensively investigated.[31−34] Moreover, recently different materials with all these characteristics including ABO3-type CaSrCuO,[35] copper sulfide CuS,[36] and Ag−In−Ni−S nanoparticles[37] etc. have been studied in trials to perform water purification under dark. These catalysts proved to be efficient for organic pollutant removal in the absence of light.

Herein, we have synthesized BFO nanoparticles and then doped them with tin (Sn) to synthesize BFSO nanoparticles. After which the BFSO nanohybrids were formed with graphene nanoplatelets (GNP) using the coprecipitation method to check the catalytic performance of these hybrids under dark and light conditions. The hybrid structures were grown in a uniform morphology and possessed stable crystal structure. It was seen that the synthesized catalysts were active under both light as well as dark conditions and showed excellent organic pollutant purification in the absence of light.

EXPERIMENTAL PROTOCOLS

Materials. Bismuth and iron nitrate salts (99% pure), tin powder, deionized water (DI), filter membrane (0.2 μm), ethylene glycol (≥99%), acetic acid (≥99.5%), graphene nanoplatelets (GNP) (A-12, Graphene Supermarket) and Congo red (commercially available) were used.

Synthesis of BFSO/GNP Nanohybrids. Ferrite salts were subjected to the sol−gel method for synthesizing BFSO nanoparticles.[22] The tin (Sn) powder was added as dopant to replace iron (Fe) atoms with a varying concentration of (5% to 25%) in a general ABO3 formula representing $BiFe_{1-x}Sn_xO_3$ where $x \approx 0.05-0.25$. The synthesized nanoparticles were named as BFSO-5 (5% Sn), BFSO-10 (10% Sn), BFSO-15 (15% Sn), BFSO-20 (20% Sn), and BFSO-25 (25% Sn), respectively. Using all the atomic weights (Bi ≈ 208 g/mol, Fe ≈ 55.8 g/mol, Sn ≈ 118 g/mol, and O ≈ 16 g/mol) and putting them into the equation $BiFe_{1-x}Sn_xO_3$ for $x = 0.05$ (5%), a 0.008 M solution of BFSO nanoparticles was prepared by immersing 2.3 mg/mL BFSO nanoparticles in a 1:1 volume ratio of ethylene glycol (EG) and acetic acid. The BFSO powder was completely dissolved inside the solvent under sonication for half hour at 65 °C as shown in Figure 1. The same method was followed for preparing solvent solutions for the rest of the Sn percentages of BFSO nanoparticles. Graphene nanoplatelets (1 mg/mL) were added to deionized water (DI) under sonication for 3 h so that the GNP clusters could make a uniform dispersion in the DI. Then both the mixtures were mixed on a hot plate with continuous stirring under 85 °C for 1 h. The chemical reaction occurred, and hybrid precipitates were allowed to settle in the solvent. When the hybrid precipitates reached room temperature, they were washed using DI water, vacuum filtered, and the final product was vacuum-dried under 70 °C for overnight.

Characterization Techniques. The synthesized hybrid structures were than subjected to crystal structure analysis with Cu−Kα X-ray DRON-8 diffractometer. JEOL JSM-6490A scanning electron microscope (SEM) was used to analyze the topography and structure morphology of hybrid structures at an accelerating voltage of 3 keV. An Escalab-250 X-ray photoelectron (XPS) spectrometer helped in studying the interface bonding of material. For catalytic activity under dark, the azo dye Congo red (CR) was dissolved at a 100 mg/L water and stirred under dark for 120 min to achieve stable solution properties. This stirring was done at a constant normal room temperature to avoid dye degradation due to thermal effects. For catalytic activity under light, the dye mixture was subjected to UV-spectrophotometer (3310 Tokyo, Japan) along with a xenon lamp of 300 W power. After every half hour of photocatalytic activity, 3 mL of solution was taken out to separate the nanohybrids via centrifugation to further check their dye removal ability.

https://doi.org/10.1021/acsomega.2c04971
ACS Omega 2023, 8, 3736−3744

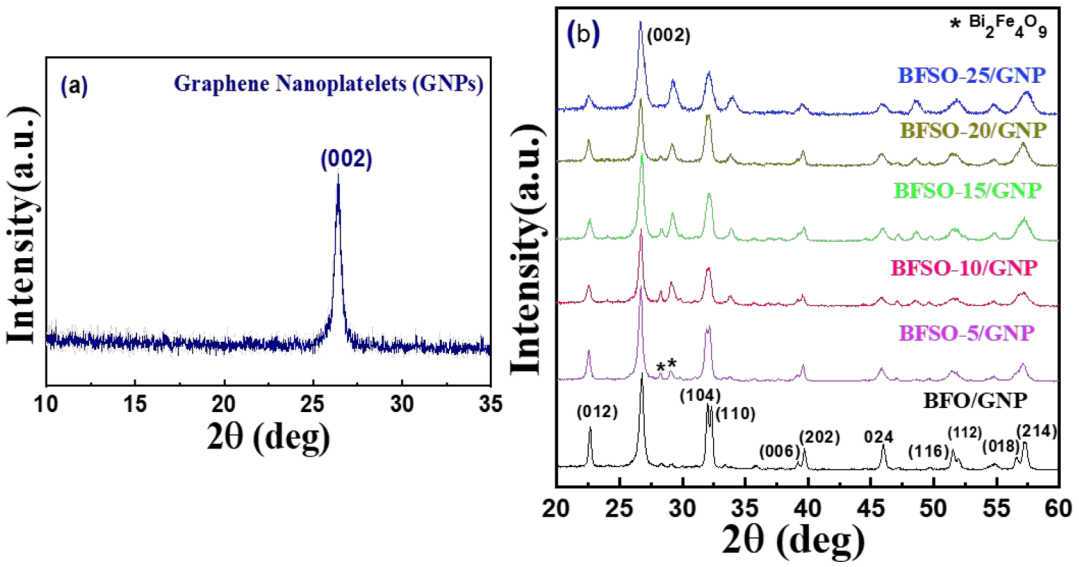

Figure 2. Illustration of XRD results of (a) graphene nanoplatelets (GNPs) and (b) BFO/GNP as well as BFSO/GNP nanohybrids with varying concentration of Sn from 5% to 25%.

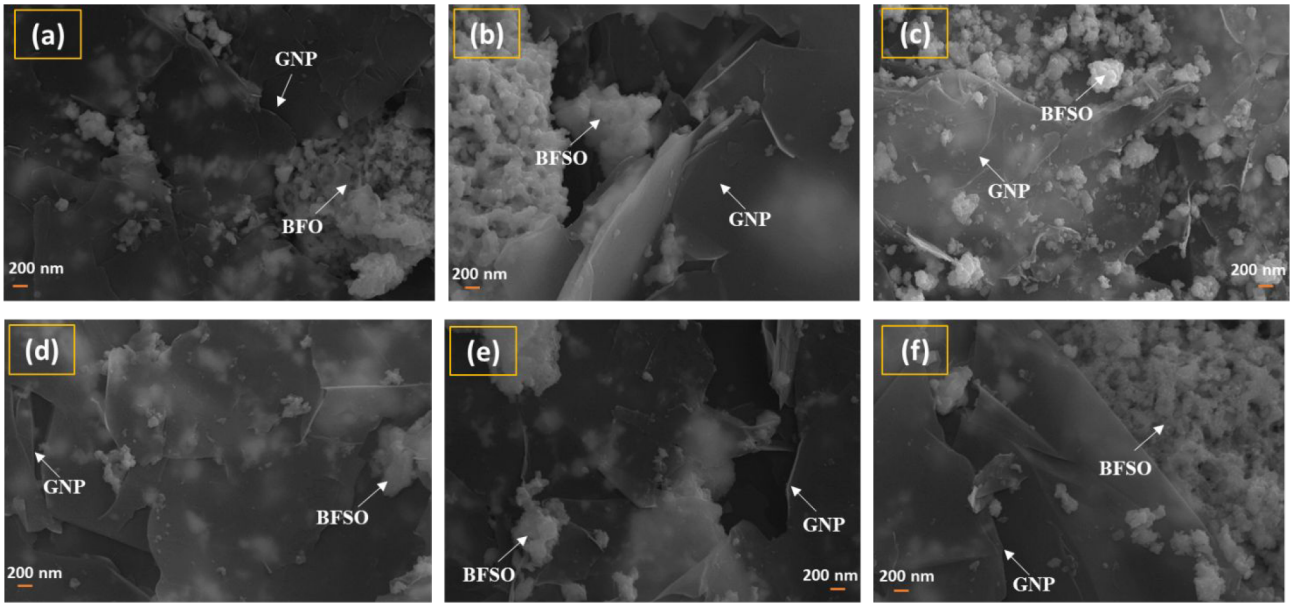

Figure 3. SEM images of (a) BFO/GNP nanohybrids along with (b–f) BFSO-5/GNP, BFSO-10/GNP, BFSO-15/GNP, BFSO-20/GNP, and BFSO-25/GNP.

RESULTS AND DISCUSSION

X-ray diffraction (XRD) analysis of graphene nanoplatelets (GNPs) is shown in Figure 2a. A peak at 26.4° can be seen inside the XRD plot corresponding to the pristine graphite structure with a (002) *hkl* plane from which the GNPs have been synthesized via thermal exfoliation process.[38] As the big three-dimensional (3D) clusters of graphite have been reduced to small platelets of 2D graphene under thermal treatment, the peak sharpness has been reduced with an increase in its width. This corresponds to a decrement in structure crystallinity with the introduction of disorder inside the sheet structure of graphene due to exfoliation.[39,40] The *d*-spacing of the GNP structure has been increased up to 3.34 Å along with the particle size of ≈35 nm. The particle size gives us the information on total number of stacked graphene sheets inside one platelet which has been estimated as 24 sheets inside one GNP. Further, in Figure 2b the XRD patterns of all the hybrids have been illustrated. Inside BFO/GNP nanohybrids a clear peak of graphene (002) plane can be seen along with all the BFO peaks verifying the presence of graphene as well as BFO particles inside the crystal structure. Moreover, all the BFO (*hkl*) faces corresponding to their diffraction angles have been mentioned inside the XRD plots. In the XRD of BFSO-5/GNP the peak doublet corresponding to (104) and (110) started merging into one single peak due to the replacement of Fe atoms with Sn.[22] The ionic size of the Sn is greater than that of Fe which causes the unit cell expansion as well as the merging of the BFO doublet inside BFSO/GNP nanohybrids. The intensity of this single peak is increased as the tin concentration increases up to 20% and then decreased inside BFSO-25/GNP due to excessive Sn loading. The width of all the peaks has been increased with the increased Sn

https://doi.org/10.1021/acsomega.2c04971
ACS Omega 2023, 8, 3736−3744

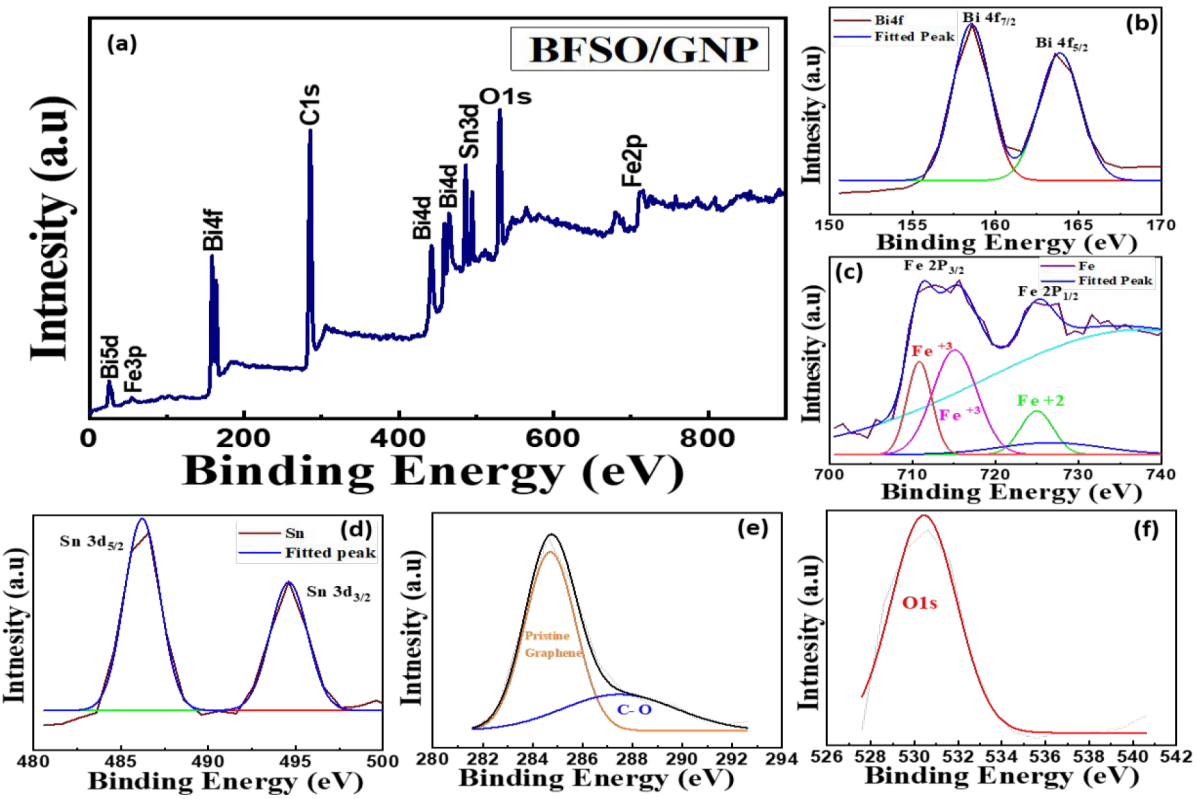

Figure 4. (a) XPS spectra of BFSO/GNP nanohybrid structure and (b–f) the deconvolution of Bi4f, Fe2p, Sn3d, C1s as well as O1s XPS peaks.

concentration. Also, the two-impurity phase that corresponds to $Bi_2Fe_4O_9$ originating from the BFO pristine phase has become prominent while moving from BFSO-5/GNP towards the BFSO-25/GNP. The increase in peak width along with the dominance of the impurity phase represents low crystallinity with increased atom disarrangement. The GNP (002) *hkl* plane is present inside all the nanohybrids along with a slight backward shift from 5% Sn to 25% Sn loading, corresponding to a further decrease in particle size of nanohybrids as compared to nanoparticles. The calculated particle size from XRD for BFO/GNP is 21.5 nm, while for BFSO-5/GNP to BFSO-25/GNP it is 23 nm, 22 nm, 20 nm, 19 nm, and 18.3 nm. Hence reduced particle size along with the structure crystallinity would make these nanohybrids more photoactive for catalysis reactions, which has already been investigated in the same type of ABO3 systems.[41]

The morphological analysis of nanohybrids is shown in SEM images presented inside Figure 3a–f at a scale of 200 nm. The dark gray sheet-like structure corresponds to the graphene sheets inside GNPs, while the white brittle clusters correlate to BFO and BFSO nanoparticles. The presence of both forms inside the SEM images is clear proof of nanohybrid formation during synthesis. In BFO/GNP and BFSO-5/GNP nanohybrids the white clusters of nanoparticles are relatively bigger while in Figure 3c–e upon increasing the tin loading from 10% to 20% the white clusters are small showing the uniform distribution of BFSO nanoparticles over graphene sheets. While again in BFSO-25/GNP the big nanoparticle clusters refer to excessive loading of Sn which is consistent with the XRD results. A transparent icy effect inside the SEM images can be seen that is due to the GNP loading inside the nanohybrids. GNPs are like a graphene flake in which few graphene sheets are stacked over one another, and with the insertion of BFSO nanoparticles over and in between these stacked sheets, a transparent icy effect in the SEM images results.[2,3]

Moreover, the X-ray photoelectron spectroscopy (XPS) analysis plot of BFSO/GNP is shown inside the Figure 4(a) to provide the information regarding compositional elements and the bonding in between these elements. All the Bi 4f, Bi 4d, and Bi 5d peaks are there to show its presence along with the Fe 2p peak.[2,42] The doping phase of tin is also present in the form of Sn 3d to show Fe^{3+} replacement with Sn^{4+}.[3,22] The presence of C 1s and O 1s peaks inside XPS further helps in analyzing the elemental bonding inside nanohybrids. The deconvolution of all the peaks related to Bi, Fe, Sn, C and O has been shown in Figure 4b–f. In the figure, bismuth Bi $4f_{7/2}$ and Bi $4f_{5/2}$ are present at 158.5 and 163.8 eV while the Fe corresponding peaks represent Fe^{2+} and Fe^{3+} at 710, 715, and 725 eV.[43] The replacement of Sn provided Sn $3d_{5/2}$ as well as Sn $3d_{3/2}$ at 486 and 495 eV (Figure 4d). The Fe^{3+} region is bonded with oxygen inside the structure, while with Sn substitution the peak corresponding to Sn $3d_{5/2}$ represented oxygen bonding inside the crystal structure.[43,44] Inside C 1s deconvolution spectra two peaks can be seen corresponding to C═C bonding due to the presence of GNPs inside the hybrid structure as well as the C−O linkage of graphene carbon structure with the BFSO nanoparticles via oxygen.[2,40] This interface bonding is further confirmed by the magnification of the O 1s peak (Figure 4f), whose existence at 531 eV is due to shifting of oxygen peak of BFSO nanoparticles from 529 eV to a forward position.[3,45] This shift occurs because of interface linkage of both structures (BFSO and GNPs) in the form of BFSO/GNP nanohybrids. The absence of any extra impurity form or oxygen containing group is a proof of impurity elimination during the careful synthesis process.

https://doi.org/10.1021/acsomega.2c04971
ACS Omega 2023, 8, 3736−3744

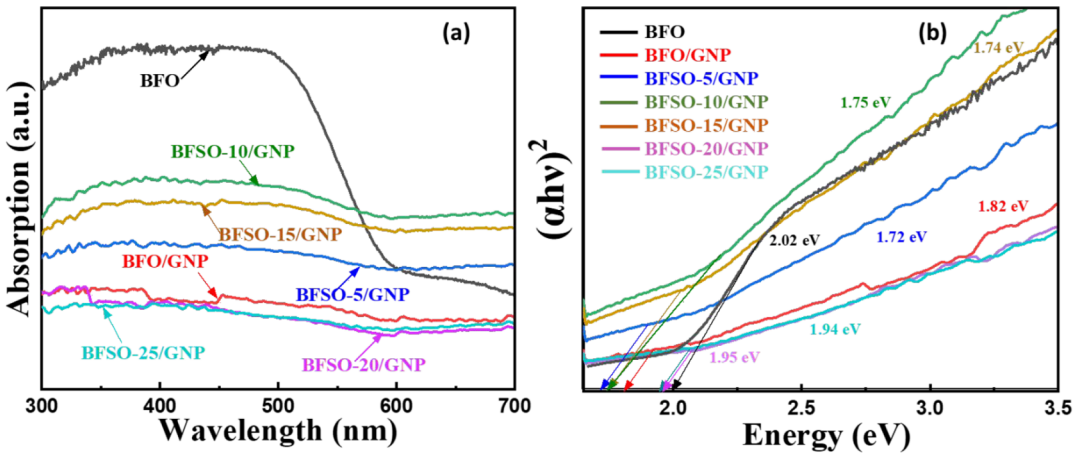

Figure 5. (a) UV−vis diffusion reflectance absorption spectra of BFO, BFO/GNP, BFSO-5/GNP, BFSO-10/GNP, BFSO-15/GNP, BFSO-20/GNP, and BFSO-25/GNP; (b) representation of Tauc plots of respective nanohybrids for band gap calculations.

The band gap analysis for the nanohybrids was also done to check whether the band gap of these structures is suitable for visible light photocatalytic activity or not. For this purpose, UV−vis diffusive reflective spectroscopy (DRS) was performed and is shown in Figure 5. The absorption for BFO is greater in the UV region but lower in the visible region as its band gap, which is approximately equal to 2.02 eV, is favorable for the UV region. While in BFO/GNP and BFSO/GNP nanohybrids the absorption is equally uniform for the whole spectral range (300 to 700 nm), which makes them favorable for the UV as well as the visible light range. Also, when the data are resolved into Tauc plots (shown in Figure 5b), it shows that with the Sn loading and GNP addition the band gap is reduced in comparison to that of BFO. The band gaps of the nanohybrids lie in between the range of 1.75 to 1.94 eV. The trend is consistent with already published studies.[3,22,42] Hence the tuning of the band gap enables the nanohybrids to absorb a broader range of light spectrum to perform as good photocatalysts.

Photoluminescence (PL) spectroscopy has also been performed, and the plots are shown in Figure 6. PL intensity gives us information regarding the charge carrier recombination and separation rates, as well as indicating photocatalytic activity.[46] The nanohybrids who have higher PL intensity have a rapid recombination rate of photocarriers during catalysis activity due to which their water purification ability is reduced in comparison to those photocatalysts who have lower PL peak intensity.[47] Graphene usually acts as an excellent charge trapping site, and its presence inside the nanohybrid will help enhance the charge carrier concentration as well as their separation rate during photocatalytic activity.[2,47] The greater is the separation in between the photocarriers, the greater is the degradation activity of the catalysts under light. So, from PL the results, the best catalysts that can perform fast under visible light are BFO/GNP and BFSO-10/GNP.

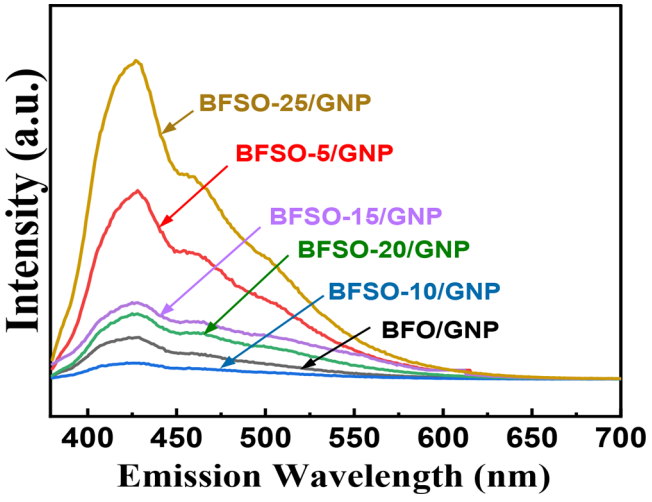

Figure 6. Photoluminescence (PL) spectra of BFO/GNP and all the BFSO/GNP nanohybrids.

The catalytic activity of the nanohybrid structures was also observed for the removal of Congo red from water, and the results are shown in Figure 7a. The dye degradation activity of the nanohybrids is higher in comparison to that of the pristine BFO (43% in 120 min) due to newly emerged energy states with Sn doping as well as graphene presence which will act as an efficient charge carrier pathway toward active sites for dye degradation. The overall dye removal for BFO/GNP nanohybrid is 62%, for BFSO-5/GNP is 22%, for BFSO-10/GNP is 42%, for BFSO-15/GNP is 100%, for BFSO-20/GNP is 56%, and for BFSO-25/GNP is 23%. It can be clearly seen that most of the nanohybrids help in half (50%) to full (100%) dye degradation during the water purification process.

This overall dye removal is accompanied by catalytic activity of nanohybrids in the presence as well as absence of light. The separated catalytic activities under visible light as well as under dark are shown inside Figure 7b. The gray portion of the bar graph corresponds to the catalytic activity under dark, while the orange portion is accompanied by the photocatalytic activity. BFSO-5/GNP and BFSO-25/GNP showed the lowest dye degradation performance including 6% to 13% dye removal under light, while accompanied by PL results. The photocatalytic activity in BFSO-10/GNP is enhanced (33%) in comparison to its catalysis under dark conditions (9%) which makes it a light active catalyst among all the nanohybrids. PL showed the lower recombination rate for BFSO-10/GNP nanohybrid in support of it to be a good photocatalyst. For BFO/GNP, BFSO-15/GNP, and BFSO-20/GNP the catalytic activity under dark is greater (32%, 89.4%, and 30%) than in light (13%, 10.6%, and 26%) which is attributed to their efficient dye removal performance even in the absence of light. Hence BFSO-15/GNP is proven to be the best catalyst for dye

https://doi.org/10.1021/acsomega.2c04971
ACS Omega 2023, 8, 3736−3744

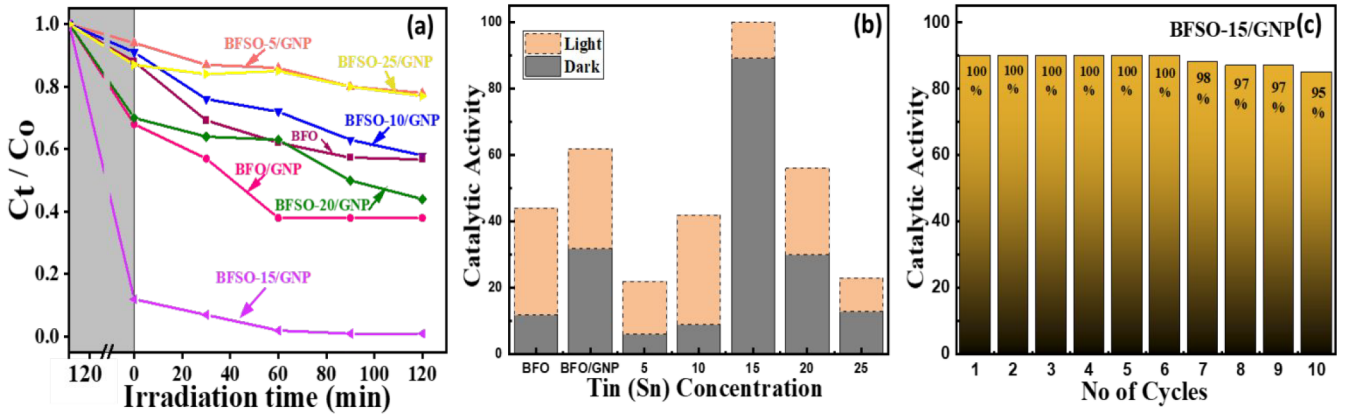

Figure 7. (a) Catalytic and photocatalytic activities of BFSO/GNP nanohybrids; (b) dye degradation abilities of BFSO/GNP catalysts under dark and light; and (c) recyclability test of BFSO-15/GNP nanohybrid.

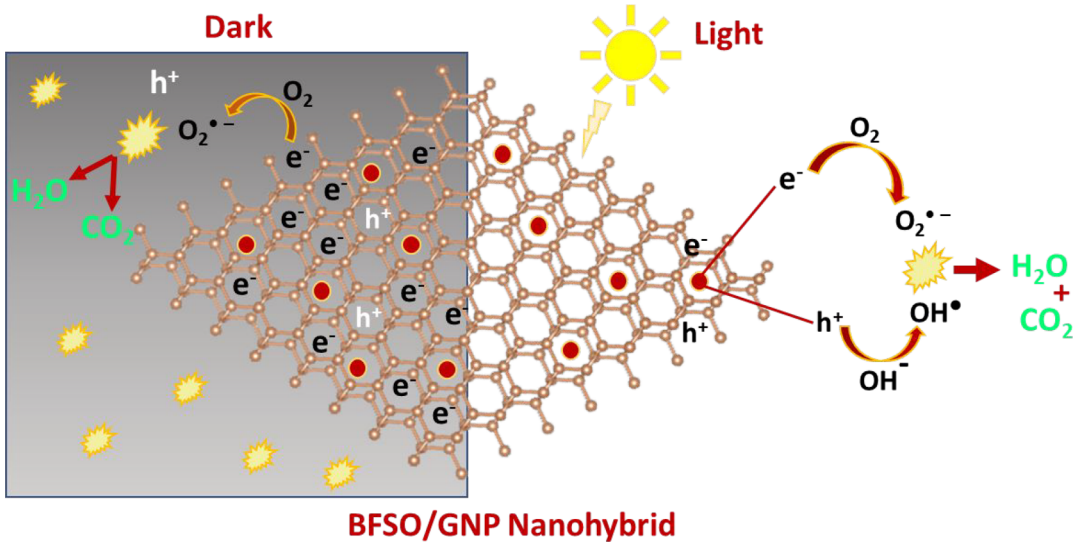

Figure 8. Illustration of dye degradation catalytic mechanism of BFSO/GNP nanohybrids under dark and light conditions.

removal as it removes 100% of organic dye under both light and dark and approximately 90% dye degradation under dark. The recyclability check was also performed to see the stability of the catalytic nanohybrid structures and their performance. It was seen that even after six cycles of catalytic activity only 2% dye degradation ability of nanohybrids was reduced as shown in Figure 7c. In addition, on reaching to the 10th cycle only 5% catalytic activity was decreased which may be due to the clogging of few active sites of nanohybrids from repeatedly performing dye degradation. Hence, as fabricated, catalytic nanohybrid species have the ability to perform exceptional dye degradation and can be used in industrial applications for organic pollutant removal even in the absence of light.

The purposed mechanism for dye degradation is shown in Figure 8. Dark GNPs in the form of platelets contain free charge carriers infused inside graphene sheet trapping states formed during the synthesis process.[35,42] Also, the doping of Sn^{4+} in replacement of Fe^{3+} will overall create holes inside the BFSO crystal structure. The electrons can easily travel through these holes as well as defect states toward the active sites of the catalyst to perform chain reactions for dye degradation.[35,36] The catalytic reactions involved in dye removal are as follows:

$$\text{catalyst}(e^-) + O_2 \rightarrow \text{catalyst} + O_2^-$$

$$O_2^- + H^+ \rightarrow HO_2^\bullet \rightarrow O_2 + H_2O_2$$

$$H_2O_2 + e^- \rightarrow OH^\bullet + OH^-$$

$$O_2^- + OH^\bullet \rightarrow \text{byproducts}$$

The oxidation reduction species ($O_2^- + OH^\bullet$) play a role in breakage of dye molecules, and at the end of this breakage harmless end products (water and carbon dioxide) are formed for further processing. In light the electrons usually get excited via light energy and the holes/electrons created in this excitation process can generate $O_2^- + OH^\bullet$ reactive species by adsorbing oxygen and reacting with water from the environment.[35−37] The generated reactive species then start oxidation reduction reactions for dye degradation to produced H_2O and CO_2 as by products.

$$\text{catalyst} + \text{light energy} \rightarrow \text{excitation} \rightarrow e^- + h^+$$

$$e^- + O_2/h^+ + H_2O \rightarrow O_2^- + OH^\bullet \rightarrow H_2O \text{ and } CO_2$$

Further the band gap structure is also analyzed in detail as shown in Figure 9. The addition of tin would create intermediate energy states under the conduction band of the

https://doi.org/10.1021/acsomega.2c04971
ACS Omega 2023, 8, 3736−3744

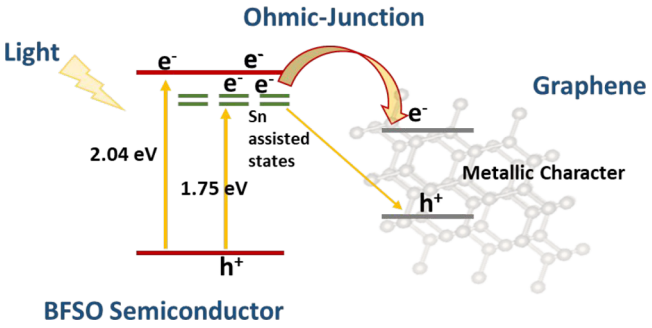

Figure 9. Illustration of ohmic-junction in between the BFSO semiconductor and metallic GNPs.

BFO. A direct Z scheme heterojunction[48,49] would be formed in between the BFSO nanoparticles and GNPs due to the metallic character of graphene. The carriers would need low energy to be excited and can move easily toward the active sites in between the ohmic junction of nanohybrids.

For showing the significance of this work a comparison has been done with already Sn based studies showed in Table 1. It

Table 1. A Comparison of Sn Doped Active Catalytic Materials with This Present Study

Active Species for Water Purification	Dye for Degradation	Photocatalytic Activity	Catalytic Activity under Dark	References
Sn doped ZnO[50]	Methylene Blue	Yes	No	50
Sn doped MoS_2	RhB	Yes	No	51
Sn doped Bi_2S_3	RhB	Yes	No	52
Sn doped Titania	Methylene Blue	Yes	Yes (10%)	53
Sn doped SnO_2	RhB	Yes	No	54
Sn doped N-doped TiO_2	Methylene Blue	Yes	No	55
Sn doped TiO_2	Methylene Blue	Yes	No	56
Sn and Gd doped BFO	Congo Red, Methylene Blue, Methylene Red	Yes	Yes (10%)	22
Sn and Gd doped BFO/GNP	Congo Red	Yes	Yes (50%)	3
Sn and Gd doped BFO/MXene	Congo Red	Yes	No	57
Sn doped BFO/GNP	Congo Red	Yes	Yes (90%)	This work

can be easily seen that most of the already reported active species for organic pollutant removal during water purification are the light driven catalysts (photocatalysts). The studies that have shown the dark activity of Sn-doped species depicted low dye degradation (50%) in comparison to this work (90%). Hence using a careful and optimized synthesis process with efficient single-element (Sn)-doped BFO/GNP nanohybrids reduced the double doping complexity during catalyst synthesis while also providing full dye removal from water in comparison to the already published results.

CONCLUSION

In summary here we have synthesized the tin (Sn) doped BFO nanoparticles (BFSO) using the sol−gel method, and then the nanohybrid structures were prepared on mixing BFSO nanoparticles with graphene nanoplatelets (GNPs) via the coprecipitation method. These BFSO/GNP nanohybrids showed good crystal structure formation with uniform phase distribution. Also, the nanohybrids proved to be efficient water purification species by possessing both catalytic as well as photocatalytic activities. It was found that the highest dye degradation ability found in BFSO-15/GNP was 100% with 90% catalytic activity under dark. Moreover, the recyclability test showed that even after 10 cycles of catalysis the nanohybrids are stable and efficient for purifying water from organic molecules. Thus, these catalytic nanohybrids stand to be remarkable candidates in the water purification field to remove organic pollutants from water under both light and dark conditions.

AUTHOR INFORMATION

Corresponding Author

Syed Rizwan − *Physics Characterization and Simulations Lab (PCSL), Department of Physics, School of Natural Sciences (SNS), National University of Sciences and Technology (NUST), Islamabad 54000, Pakistan;* orcid.org/0000-0002-6934-0949; Email: syedrizwan@sns.nust.edu.pk, syedrizwanh83@gmail.com

Author

Sabeen Fatima − *Physics Characterization and Simulations Lab (PCSL), Department of Physics, School of Natural Sciences (SNS), National University of Sciences and Technology (NUST), Islamabad 54000, Pakistan;* orcid.org/0000-0001-7173-1490

Complete contact information is available at: https://pubs.acs.org/10.1021/acsomega.2c04971

Author Contributions

Sabeen Fatima performed synthesis, experimentation and paper writing and Syed Rizwan supervised the complete project.

Notes

The authors declare no competing financial interest.

ACKNOWLEDGMENTS

The authors thank the Higher Education Commission (HEC) of Pakistan for providing research funding under the Project No: 20-14784/NRPU/R&D/HEC/2021.

REFERENCES

(1) Amin, M. T.; Alazba, A. A.; Manzoor, U. A Review of Removal of Pollutants from Water/Wastewater Using Different Types of Nanomaterials. *Adv. Mater. Sci. Eng.* **2014**, *2014*, 1.

(2) Fatima, S.; Ali, S. I.; Iqbal, M. Z.; Rizwan, S. The High Photocatalytic Activity and Reduced Band Gap Energy of La and Mn Co-Doped BiFeO3/Graphene Nanoplatelet (GNP) Nanohybrids. *RSC Adv.* **2017**, *7* (57), 35928−35937.

(3) Fatima, S.; Ali, S. I.; Iqbal, M. Z. Congo Red Dye Degradation by Graphene Nanoplatelets/Doped Bismuth Ferrite Nanoparticle Hybrid Catalysts under Dark and Light Conditions. *Catalysts* **2020**, *10*, 367.

(4) Freitag, M.; Möller, N.; Rühling, A.; Strassert, C. A.; Ravoo, B. J.; Glorius, F. Photocatalysis in the Dark: Near-Infrared Light Driven

Photoredox Catalysis by an Upconversion Nanoparticle/Photocatalyst System. *ChemPhotoChem.* **2019**, *3* (1), 24−27.
(5) Cai, J.; Shen, J.; Zhang, X.; Ng, Y. H.; Huang, J.; Guo, W.; Lin, C.; Lai, Y. Light-Driven Sustainable Hydrogen Production Utilizing TiO2 Nanostructures: A Review. *Small Methods* **2019**, *3* (1), 1−24.
(6) Vijayan, B.; Dimitrijevic, N. M.; Rajh, T.; Gray, K. Effect of Calcination Temperature on the Photocatalytic Reduction and Oxidation Processes of Hydrothermally Synthesized Titania Nanotubes. *J. Phys. Chem. C* **2010**, *114* (30), 12994−13002.
(7) López-de-Alba, P. L.; López-Martínez, L.; De-León-Rodríguez, L. M. Simultaneous Determination of Synthetic Dyes Tartrazine, Allura Red and Sunset Yellow by Differential Pulse Polarography and Partial Least Squares. A Multivariate Calibration Method. *Electroanalysis* **2002**, *14* (3), 197−205.
(8) Ramsay, R. R.; Dunford, C.; Gillman, P. K. Methylene Blue and Serotonin Toxicity: Inhibition of Monoamine Oxidase A (MAO A) Confirms a Theoretical Prediction. *Br. J. Pharmacol.* **2007**, *152* (6), 946−951.
(9) Afkhami, A.; Moosavi, R. Adsorptive Removal of Congo Red, a Carcinogenic Textile Dye, from Aqueous Solutions by Maghemite Nanoparticles. *J. Hazard. Mater.* **2010**, *174* (1−3), 398−403.
(10) Umar, M.; Mahmood, N.; Awan, S. U.; Fatima, S.; Mahmood, A.; Rizwan, S. Rationally Designed La and Se Co-Doped Bismuth Ferrites with Controlled Bandgap for Visible Light Photocatalysis. *RSC Adv.* **2019**, *9* (30), 17148−17156.
(11) Zhang, N.; Chen, D.; Niu, F.; Wang, S.; Qin, L.; Huang, Y. Enhanced Visible Light Photocatalytic Activity of Gd-Doped BiFeO3 Nanoparticles and Mechanism Insight. *Sci. Rep.* **2016**, *6* (May), 1−11.
(12) An, J.; Zhu, L.; Wang, N.; Song, Z.; Yang, Z.; Du, D.; Tang, H. Photo-Fenton like Degradation of Tetrabromobisphenol A with GrapheneBiFeO3 Composite as a Catalyst. *Chem. Eng. J.* **2013**, *219*, 225−237.
(13) Wang, J.; Neaton, J. B.; Zheng, H.; Nagarajan, V.; Ogale, S. B.; Liu, B.; Viehland, D.; Vaithyanathan, V.; Schlom, D. G.; Waghmare, U. V.; Spaldin, N. A.; Rabe, K. M.; Wuttig, M.; Ramesh, R. Epitaxial BiFeO3Multiferroic Thin Film Heterostructures. *Science (80-.).* **2003**, *299* (5613), 1719−1722.
(14) Vijayasundaram, S. V.; Suresh, G.; Mondal, R. A.; Kanagadurai, R. Substitution-Driven Enhanced Magnetic and Ferroelectric Properties of BiFeO3 Nanoparticles. *J. Alloys Compd.* **2016**, *658*, 726−731.
(15) Wang, N.; Luo, X.; Han, L.; Zhang, Z.; Zhang, R.; Olin, H.; Yang, Y. Structure, Performance, and Application of BiFeO3 Nanomaterials. *Nano-Micro Lett.* **2020**, *12* (1), 420 DOI: 10.1007/s40820-020-00420-6.
(16) Wu, H.; Zhou, J.; Liang, L.; Li, L.; Zhu, X. Fabrication, Characterization, Properties, and Applications of Low-Dimensional BiFeO 3 Nanostructures. *J. Nanomater.* **2014**, *2014*, 1.
(17) Gao, F.; Chen, X.; Yin, K.; Dong, S.; Ren, Z.; Yuan, F.; Yu, T.; Zou, Z.; Liu, J. M. Visible-Light Photocatalytic Properties of Weak Magnetic BiFeO3 Nanoparticles. *Adv. Mater.* **2007**, *19* (19), 2889−2892.
(18) Haruna, A.; Abdulkadir, I.; Idris, S. O. Photocatalytic Activity and Doping Effects of BiFeO3 Nanoparticles in Model Organic Dyes. *Heliyon* **2020**, *6* (1), No. e03237.
(19) Papadas, I.; Christodoulides, J. A.; Kioseoglou, G.; Armatas, G. S. A High Surface Area Ordered Mesoporous BiFeO3 Semiconductor with Efficient Water Oxidation Activity. *J. Mater. Chem. A* **2015**, *3* (4), 1587−1593.
(20) Yang, Q.; Xu, Q.; Sobhan, M.; Ke, Q.; Anariba, F.; Ong, K. P.; Wu, P. Simultaneous Reduction in Leakage Current and Enhancement in Magnetic Moment in BiFeO3 Nanofibers via Optimized Sn Doping. *Phys. Status Solidi - Rapid Res. Lett.* **2014**, *8* (7), 653−657.
(21) Sobhan, M.; Xu, Q.; Zhao, J.; Franklin, A.; Hu, Y.; Tse, J. S.; Wu, P. Modification of Surface Chemistry by Lattice Sn Doping in BiFeO3 Nanofibers. *Epl* **2015**, *111* (1), 18005.
(22) Irfan, S.; Rizwan, S.; Shen, Y.; Li, L.; Asfandiyar; Butt, S.; Nan, C. W. The Gadolinium (Gd3+) and Tin (Sn4+) Co-Doped BiFeO3 Nanoparticles as New Solar Light Active Photocatalyst. *Sci. Rep.* **2017**, *7* (August 2016), 1−12.
(23) Li, Z.; Shen, Y.; Guan, Y.; Hu, Y.; Lin, Y.; Nan, C. W. Bandgap Engineering and Enhanced Interface Coupling of Graphene-BiFeO 3 Nanocomposites as Efficient Photocatalysts under Visible Light. *J. Mater. Chem. A* **2014**, *2* (6), 1967−1973.
(24) Wang, X.; Mao, W.; Wang, Q.; Zhu, Y.; Min, Y.; Zhang, J.; Yang, T.; Yang, J.; Li, X.; Huang, W. Low-Temperature Fabrication of Bi25FeO40/RGO Nanocomposites with Efficient Photocatalytic Performance under Visible Light Irradiation. *RSC Adv.* **2017**, *7* (17), 10064−10069.
(25) Li, T.; Shen, J.; Li, N.; Ye, M. Hydrothermal Preparation, Characterization and Enhanced Properties of Reduced Graphene-BiFeO3 Nanocomposite. *Mater. Lett.* **2013**, *91*, 42−44.
(26) Sun, A.; Chen, H.; Song, C.; Jiang, F.; Wang, X.; Fu, Y. Magnetic Bi25FeO40-Graphene Catalyst and Its High Visible-Light Photocatalytic Performance. *RSC Adv.* **2013**, *3* (13), 4332−4340.
(27) Zheng, L.; Han, S.; Liu, H.; Yu, P.; Fang, X. Hierarchical MoS2 Nanosheet@TiO2 Nanotube Array Composites with Enhanced Photocatalytic and Photocurrent Performances. *Small* **2016**, *12* (11), 1527−1536.
(28) Gao, N.; Fang, X. Synthesis and Development of Graphene-Inorganic Semiconductor Nanocomposites. *Chem. Rev.* **2015**, *115* (16), 8294−8343.
(29) Liu, S.; Zheng, L.; Yu, P.; Han, S.; Fang, X. Novel Composites of α-Fe2O3 Tetrakaidecahedron and Graphene Oxide as an Effective Photoelectrode with Enhanced Photocurrent Performances. *Adv. Funct. Mater.* **2016**, *26* (19), 3331−3339.
(30) Han, S.; Hu, L.; Liang, Z.; Wageh, S.; Al-Ghamdi, A. A.; Chen, Y.; Fang, X. One-Step Hydrothermal Synthesis of 2D Hexagonal Nanoplates of α-Fe2O3/Graphene Composites with Enhanced Photocatalytic Activity. *Adv. Funct. Mater.* **2014**, *24* (36), 5719−5727.
(31) Yu, Q.; Chen, J.; Li, Y.; Wen, M.; Liu, H.; Li, G.; An, T. In-Situ Decoration of Metallic Bi on BiOBr with Exposed (110) Facets and Surface Oxygen Vacancy for Enhanced Solar Light Photocatalytic Degradation of Gaseous n-Hexane. *Chin. J. Catal.* **2020**, *41* (10), 1603−1612.
(32) Chen, Y. L.; Xu, Y. X.; Lin, D. F.; Luo, Y. J.; Xue, H.; Chen, Q. H. Insight into Superior Visible Light Photocatalytic Activity for Degradation of Dye over Corner-Truncated Cubic Ag2O Decorated TiO2 Hollow Nanofibers. *Jiegou Huaxue* **2020**, *39* (3), 588−597.
(33) Li, S.; Cai, M.; Liu, Y.; Zhang, J.; Wang, C.; Zang, S.; Li, Y.; Zhang, P.; Li, X. In-situ constructing C3N5 nanosheets/Bi2WO6 nanodots S-scheme heterojunction with enhanced structural defects for efficiently photocatalytic removal of tetracycline and Cr(VI). *Inorg. Chem. Front.* **2022**, *9*, 2479−2497.
(34) Long, Z.; Xian, G.; Zhang, G.; Zhang, T.; Li, X. BiOCl-Bi12O17Cl2 Nanocomposite with High Visible-Light Photocatalytic Activity Prepared by an Ultrasonic Hydrothermal Method for Removing Dye and Pharmaceutical. *Chin. J. Catal.* **2020**, *41* (3), 464−473.
(35) Chen, H.; Ku, J.; Wang, L. Thermal Catalysis under Dark Ambient Conditions in Environmental Remediation: Fundamental Principles, Development, and Challenges. *Chin. J. Catal.* **2019**, *40* (8), 1117−1134.
(36) Ma, Y.; Zhang, J.; Wang, Y.; Chen, Q.; Feng, Z.; Sun, T. Concerted Catalytic and Photocatalytic Degradation of Organic Pollutants over CuS/g-C 3 N 4 Catalysts under Light and Dark Conditions. *J. Adv. Res.* **2019**, *16*, 135−143.
(37) Molla, A.; Sahu, M.; Hussain, S. Under Dark and Visible Light: Fast Degradation of Methylene Blue in the Presence of Ag-In-Ni-S Nanocomposites. *J. Mater. Chem. A* **2015**, *3* (30), 15616−15625.
(38) Guerra, V.; Wan, C.; Degirmenci, V.; Sloan, J.; Presvytis, D.; Watson, M.; McNally, T. Characterisation of Graphite Nanoplatelets (GNP) Prepared at Scale by High-Pressure Homogenisation. *J. Mater. Chem. C* **2019**, *7* (21), 6383−6390.
(39) Hamidinejad, S. M.; Chu, R. K. M.; Zhao, B.; Park, C. B.; Filleter, T. Enhanced Thermal Conductivity of Graphene Nanoplatelet-Polymer Nanocomposites Fabricated via Supercritical Fluid-Assisted in Situ Exfoliation. *ACS Appl. Mater. Interfaces* **2018**, *10* (1), 1225−1236.

https://doi.org/10.1021/acsomega.2c04971
ACS Omega 2023, 8, 3736−3744

(40) Batakliev, T.; Petrova-Doycheva, I.; Angelov, V.; Georgiev, V.; Ivanov, E.; Kotsilkova, R.; Casa, M.; Cirillo, C.; Adami, R.; Sarno, M.; Ciambelli, P. Effects of Graphene Nanoplatelets and Multiwall Carbon Nanotubes on the Structure and Mechanical Properties of Poly(Lactic Acid) Composites: A Comparative Study. *Appl. Sci.* **2019**, *9* (3), 469.
(41) Zhang, Y.; Zhao, X.; Chen, J.; Li, S.; Yang, W.; Fang, X. Self-Polarized BaTiO3 for Greatly Enhanced Performance of ZnO UV Photodetector by Regulating the Distribution of Electron Concentration. *Adv. Funct. Mater.* **2020**, *30* (5), 1−9.
(42) Fatima, S.; Ali, S. I.; Younas, D.; Islam, A.; Akinwande, D.; Rizwan, S. Graphene Nanohybrids for Enhanced Catalytic Activity and Large Surface Area. *MRS Commun.* **2019**, *9* (1), 27−36.
(43) Zhang, Y.; Wang, Y.; Qi, J.; Tian, Y.; Zhang, J.; Wei, M.; Liu, Y.; Yang, J. Structural, Magnetic and Impedance Spectroscopy Properties of Ho 3+ Modified BiFeO 3 Multiferroic Thin Film. *J. Mater. Sci. Mater. Electron.* **2019**, *30* (3), 2942−2952.
(44) Costa, I. M.; Colmenares, Y. N.; Pizani, P. S.; Leite, E. R.; Chiquito, A. J. Sb Doping of VLS Synthesized SnO2 Nanowires Probed by Raman and XPS Spectroscopy. *Chem. Phys. Lett.* **2018**, *695*, 125−130.
(45) Iqbal, M. A.; Ali, S. I.; Amin, F.; Tariq, A.; Iqbal, M. Z.; Rizwan, S. La-and Mn-Codoped Bismuth Ferrite/Ti 3 C 2 MXene Composites for Efficient Photocatalytic Degradation of Congo Red Dye. *ACS Omega* **2019**, *4* (5), 8661−8668.
(46) Arshad, A.; Iqbal, J.; Siddiq, M.; Mansoor, Q.; Ismail, M.; Mehmood, F.; Ajmal, M.; Abid, Z. Graphene Nanoplatelets Induced Tailoring in Photocatalytic Activity and Antibacterial Characteristics of MgO/Graphene Nanoplatelets Nanocomposites. *J. Appl. Phys.* **2017**, *121* (2), 024901.
(47) Worajittiphon, P.; Pingmuang, K.; Inceesungvorn, B.; Wetchakun, N.; Phanichphant, S. Enhancing the Photocatalytic Activity of ZnO Nanoparticles for Efficient Rhodamine B Degradation by Functionalised Graphene Nanoplatelets. *Ceram. Int.* **2015**, *41* (1), 1885−1889.
(48) He, R.; Chen, R.; Luo, J.; Zhang, S.; Xu, D. Fabrication of Graphene Quantum Dots Modified Bioi/Pan Flexible Fiber with Enhanced Photocatalytic Activity. *Acta Phys. - Chim. Sin.* **2021**, *37* (6), 2011022.
(49) He, K.; Shen, R.; Hao, L.; Li, Y.; Zhang, P.; Jiang, J.; Xin, L. Advances in Nanostructured Silicon Carbide Photocatalysts. *Acta Phys. Chim. Sin.* **2022**, *0* (0), 0−0.
(50) Siva, N.; Sakthi, D.; Ragupathy, S.; Arun, V.; Kannadasan, N. Synthesis, Structural, Optical and Photocatalytic Behavior of Sn Doped ZnO Nanoparticles. *Mater. Sci. Eng. B Solid-State Mater. Adv. Technol.* **2020**, *253* (January), 114497.
(51) Nandigana, P.; Mahato, S.; Dhandapani, M.; Pradhan, B.; Subramanian, B.; Panda, S. K. Lyophilized Tin-Doped MoS2 as an Efficient Photocatalyst for Overall Degradation of Rhodamine B Dye. *J. Alloys Compd.* **2022**, *907*, 164470.
(52) Jiang, Y.; Hu, J.; Li, J. Synthesis and Visible Light Responsed Photocatalytic Activity of Sn Doped Bi2S3Microspheres Assembled by Nanosheets. *RSC Adv.* **2016**, *6* (46), 39810−39817.
(53) Bhange, P. D.; Awate, S. V.; Gholap, R. S.; Gokavi, G. S.; Bhange, D. S. Photocatalytic Degradation of Methylene Blue on Sn-Doped Titania Nanoparticles Synthesized by Solution Combustion Route. *Mater. Res. Bull.* **2016**, *76*, 264−272.
(54) Letifi, H.; Dridi, D.; Litaiem, Y.; Ammar, S.; Dimassi, W.; Chtourou, R. High Efficient and Cost Effective Titanium Doped Tin Dioxide Based Photocatalysts Synthesized via Co-Precipitation Approach. *Catalysts* **2021**, *11* (7), 803.
(55) Panghulan, G. R.; Vasquez, M. R.; Edañol, Y. D.; Chanlek, N.; Payawan, L. M. Synthesis of TiN/N-Doped TiO 2 Composite Films as Visible Light Active Photocatalyst. *J. Vac. Sci. Technol. B* **2020**, *38* (6), 062203.
(56) Zhou, X.; Lu, J.; Li, L.; Wang, Z. Preparation of Crystalline Sn-Doped TiO2 and Its Application in Visible-Light Photocatalysis. *J. Nanomater.* **2011**, *2011*, 432947.
(57) Tariq, A.; Ali, S. I.; Akinwande, D.; Rizwan, S. Efficient Visible-Light Photocatalysis of 2D-MXene Nanohybrids with Gd3+- and Sn4+-Codoped Bismuth Ferrite. *ACS Omega* **2018**, *3* (10), 13828−13836.

https://doi.org/10.1021/acsomega.2c04971
ACS Omega 2023, 8, 3736−3744